BED-Vol. 22, Advances in Bioengineering
ASME 1992

PRESSURE DROP IN A TAPERED FEMORAL ARTERY OF A DOG: PULSATILE FLOW

Rupak K. Banerjee, Young I. Cho
Department of Mechanical Engineering and Mechanics
Drexel University, Philadelphia, PA 19104

Lloyd H. Back
Jet Propulsion Laboratory
California Institute of Technology, Pasadena, CA 91109

ABSTRACT

The study is aimed at the numerical prediction of pressure drop using the *in-vivo* pulsatile velocity obtained in the femoral artery of a living dog with a heart rate of 128 beats/min. Knowing the *in-vivo* velocity pulse by any non-invasive method, the physiological pressure drop may be predicted for any normal or diseased artery. The prediction of *in-vivo* pressure drop is within the two limits of ·ut flow conditions: uniform and parabolic. Temporal and spatial ations of flow parameters, i.e., velocity profile, shear rate, non-·wtonian viscosity, and wall shear stress are reported to validate the pressure numerical procedure. There exist both positive and negative shear rates during a pulse cycle, in other words, the wall experiences zero shear twice during a cycle. Taper of artery not only increases the magnitude of the positive and negative shear rates but causes a steep gradient in shear rate, which in turn affects wall shear stress and pressure.

INTRODUCTION

The objective of this study is to calculate instantaneous pressure drop using *in-vivo* velocity wave in a mildly tapered femoral artery of a dog and to predict the pressure drop along the axial direction. Instantaneous inlet velocity may be measured in a living being by a non-invasive method, e.g., Doppler flow meter, magnetic resonance imaging technique or any other tool. In order to discuss the pressure drop at the wall, the temporal and spatial variations of velocity profile, shear rate, non-Newtonian viscosity, and wall shear stress need to be addressed.

Flow reversal in the dog's artery and phase lag between pressure gradient and flow were not only reported by McDonald and his co-workers [1] but numerically studied by Womersley [2]. Ling et. al. [3] reported that, for dog's aorta, flow profiles were found to develop locally and transiently during the passage of pressure-gradient wave. *In-vivo* velocity and shear rate data, in their studies, indicated relatively flat velocity profiles. Back et. al. [4] measured *in-vitro* pulsatile velocity and pressure in a human femoral artery model with reverse lumen curvature. Talbot and Burger [5] illustrated the relation of acceleration and deceleration of velocity to pressure distribution along with useful discussion on fluid-mechanical aspects of blood circulation. The measured non-Newtonian properties, i.e., shear thinning and viscoelasticity, of blood have been reported by Mann and Tarbell [6], and Liepsch and ırston [7]. Cho and Kensey [8] and Banerjee et. al. [9] reported ımportance of non-Newtonian properties of blood in flow ѕimulations. Although various authors have reported experimental and numerical procedures to obtain pressure-flow relationship, the numerical prediction of *in-vivo* pressure drop using Navier-Stokes equations with the convective terms in an arterial geometry having physiological shape have not been documented in full.

METHODS

Geometry of the dog's femoral artery has been redrawn from the angiogram as shown in Fig. 1A. The pressure drop across the mildly tapered segment is numerically calculated between small branch arteries denoted by port No. 1 and 2. *In-vivo* pressure drop

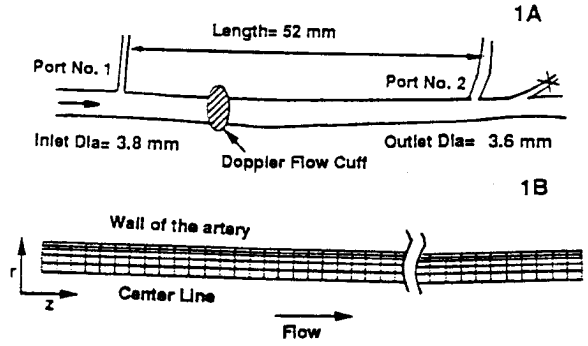

FIG. 1 X-ray tracing of femoral artery of a living dog (Fig. 1A). Ligated small branch arteries are marked port No. 1 and 2. The mesh plot of the femoral artery is shown in Fig 1B.

measurements across these ligated arteries [port No. 1 and 2], connected to the tubing leading to the transducer, will be reported elsewhere. As shown in Fig. 1A, the flow cuff for the Doppler flow meter was located near the first pressure port.

Using a Finite Element Method (FEM), Galerkin formulation [10] is applied to discretize the continuity and momentum equations. A matrix equation representing the discrete analog of the original equations for an individual fluid element was constructed, assembled, and solved using standard solution procedures [11]. The mesh plot for the artery is shown in Fig. 1B. In comparison to the core elements of the artery the element sizes near the wall are kept smaller to achieve a better accuracy of flow parameters. The aspect ratio of 9-nodal quadrilateral elements was chosen to be less than 10. The numerical simulation of a pulsatile flow requires a time integration method. The implicit time integration scheme used in the

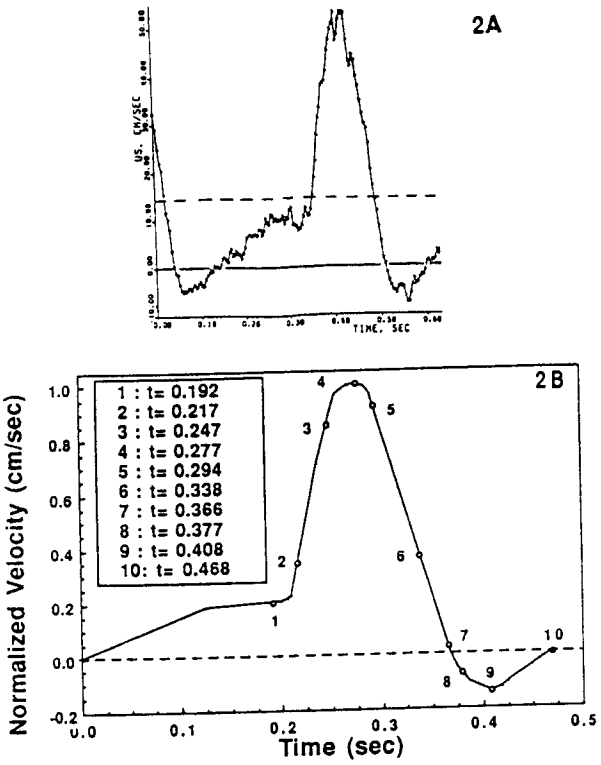

FIG. 2 The *in-vivo* velocity near the core of the femoral artery along a pulse cycle obtained by Doppler Flow Cuff (Fig. 2A). Normalized form of the *in-vivo* velocity pulse along with the time steps for which flow data are reported in the present paper(Fig. 2B).

current study is the second order trapezoidal method with a variable time step, which depends on the magnitude of temporal velocity and its gradient change. For spatial integration, the number of iteration steps is limited to ten at each time step with a combination of the successive substitution and Quasi-Newton scheme.

No-slip boundary condition has been specified on the rigid arterial wall. Compliance of the artery is neglected for the present study since a factor of only 0.6% compliance has been reported for the femoral artery of dog [1]. Figure 2A shows the *in-vivo* velocity profile at the core region measured by a ultrasound Doppler flow cuff. The inlet velocity profile has been normalized as shown in Fig. 2B, and used as an input for the numerical simulation. The selected time steps for flow analysis have been marked from No.1 to No.10 on the pulse. By a non-invasive method it is difficult to obtain an accurate *in-vivo* instantaneous velocity inlet profile, which could either be parabolic, uniform or any intermediate of the two. Hence, both the extreme cases, i.e., parabolic and uniform velocity profiles, have been considered as input at the inlet.

In the present investigation, the Wilburn and Schneck's Best Three Variable Model (B3VM) of the whole blood [12] has been used to represent the non-Newtonian blood viscosity (η) where model constants are obtained by a multiple regression technique performed on viscometric data of anticoagulated blood samples of known hematocrit and chemical composition.

$$\eta = A[\, e^{B*H}][e^{D(T/(H\hat{}2))}]\,[\dot{\gamma}^{-C*H}] \qquad (1)$$

where $A = 0.00797\ P(sec)^{-D*H}$; $B = 0.0608$;
$C = 0.00499$; $D = 145.85$ dl./g.;
H= Hematocrit %; T = TPMA gm/100ml;

$\dot{\gamma}$= shear rate;

In general, the whole blood model has been used to determine the viscosity of human blood. At 37°C, the viscosities of human and dog blood are almost identical [13]. Hematocrit of 44% and TPMA (Total Protein minus Albumin, essentially the globulins and fibrinogens) of 3.51 gm/100ml have been reported for dog's blood [13], and these values are incorporated in the present blood model.

In order to calculate viscosity in the flow field locally, the local shear rate, $\dot{\gamma}$, is calculated from velocity gradient through the second invariant of the rate of strain tensor, $II_{\dot{\gamma}}$, as follows:

$$\dot{\gamma} = \sqrt{\frac{1}{2}\Pi} = \sqrt{\frac{1}{2}\left[\sum_i \sum_j \dot{\gamma}_{ij}\,\dot{\gamma}_{ji}\right]} \qquad (2)$$

After the local viscosity is determined by the whole blood model, Eq. (1), the local shear stress, τ ($= \eta\,\dot{\gamma}$), is calculated.

Of note is that the pressure term in the momentum equation is replaced using velocity vectors using different types of penalty formulation [10,11]. Often the FEM is not directly applied to a system of equations but rather to a perturbed system of equations in which the continuity requirement is weakened and replaced by

$$u_{i,j} = -\varepsilon p \qquad \text{where } \varepsilon = 10^{-9} \qquad (3)$$

For a high aspect ratio of the elements, a small penalty parameter is recommended. Physically, this can be equated to simulating the flow having insignificant compressibility effect. This approach has the advantage of eliminating one of the dependent variables, pressure, which is then recovered during post-processing from the velocity field by

$$p^{\varepsilon} = -u_i^{\varepsilon}{}_{,i} / \varepsilon \qquad (4)$$

In particular, the use of the pressure penalty method requires that an implicit time integration scheme be used for the solution of such an unsteady problem. The finite-element computer code FIDAP is used to formulate and solve the matrix equation on the IBM-3090.

RESULTS AND DISCUSSIONS

Detailed flow analysis is presented for the discontinuous linear formulation (of pressure) with global basis function. Figure 3A represents the velocity profile at port No.1. The systolic acceleration is represented by curves 1-4 whereas deceleration is represented by curves 5-7. The exact time corresponding to the number of curve can be seen in Fig. 2B, which shows that the input velocity at the inlet is positive for curves 1-7. The instantaneous velocity profiles of curves 1-6 are positive in nature whereas for curve 7 a flow reversal is obtained near the wall, though the core velocity is positive. Flow reversal near the wall during the late decelerating flow of a positive systolic velocity is an interesting phenomenon.

For port No.2 (Fig. 3B) similar observations have been noted with expected variations of velocity caused by the mild taper. Due to the gradual taper of the artery, at port No.2 a less parabolic or, in other words, a more blunt velocity profile is obtained with a reduced peak value. Furthermore, in comparison to port No.1, curve 7 for port No.2 shows a higher value of reversed peak flow and an extended flow reversal zone near the arterial wall. Instantaneous velocity profiles obtained during diastole are represented by curves 8-10 for which the input inlet velocity is negative. For accelerating negative flow, curves 8-9, the negative flow near the wall is greater in magnitude than at the core. This indicates that during late systole and early diastole the wall region experiences a faster and greater change of velocity and its gradient. A similar observation is noted at late diastole (deceleration of negative flow), curve 10, where the core velocity is negative in comparison to a positive velocity near the wall. Curves 9-10 indicate transitions from a peak negative diastolic flow to a positive flow. For port No.2 the effect of the taper of the artery is magnified and, hence, the velocity gradient at the wall for port No.2 is larger than for port No.1.

Along a single cardiac pulse, an oscillating wall shear may be observed in Figs. 4A-4C. For port No.1 (Fig. 4A) the shear rate varies from a zero value to a maximum positive value of 420 sec^{-1} (at maximum acceleration before peak systolic, time step 3) and attains a zero shear rate during the decelerating phase of late systole (between time step 6 and 7) before reaching a maximum negative shear rate of -90 sec^{-1} (early diastole, acceleration of negative velocity at time step 8) which is followed by a shear rate of 15 sec^{-1} at the end of reverse flow. For port No.2 (Fig. 4B) the shear rate varies from a zero value to a maximum positive value of 668 sec^{-1} and attains a zero shear

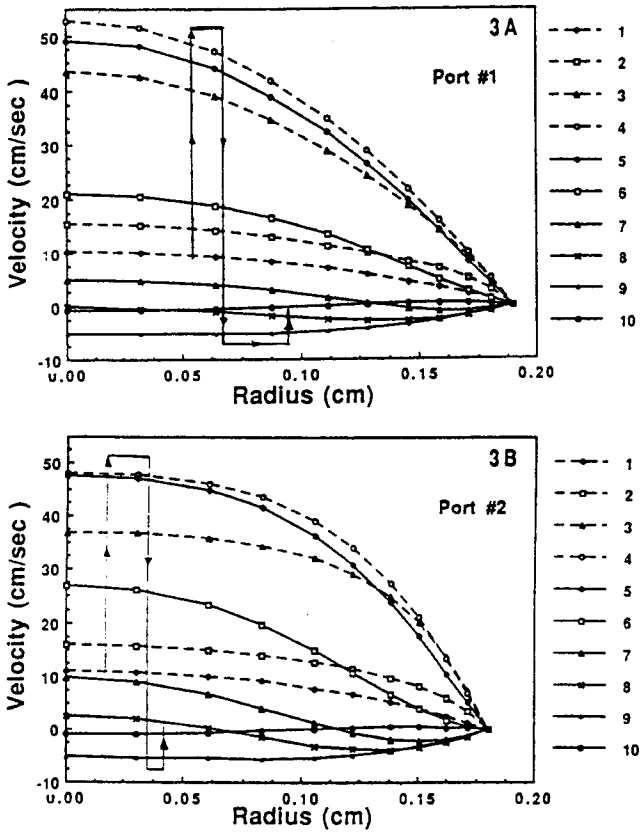

FIG. 3 Radial velocity distribution for different time steps along a pulse cycle at port No. 1 (Fig. 3A) and at port No. 2 (Fig. 3B).

rate value during the decelerating phase of the late systole before reaching a maximum negative shear rate of -127 sec^{-1}, which is followed by a shear rate of 17 sec^{-1} at the end of reverse flow. A steeper gradient in the wall shear rate due to the taper is observed during both acceleration and deceleration for port No.2 than for port No.1. This in turn affects the non-Newtonian viscosity, shear stress, and pressure drop. The systolic decelerating slope of the shear rate at port No.2 is higher than at port No.1, causing the lines to intersect between the time steps 5 and 6 (Fig. 4C), an interesting phenomenon. The wall shear rates during deceleration significantly change with taper. The significant observation is the existence of wall shear which oscillates between positive and negative values during a single cardiac cycle. Furthermore, a change in wall geometry, e.g., the taper of the arterial wall, significantly affects the wall shear rate.

The non-Newtonian viscosity is obtained from the whole blood model based on the magnitude of shear rate. The non-Newtonian viscosity at the wall is presented in Fig. 5. It is apparent that for high shear, the non-Newtonian viscosity is low and vice-versa. In general, the shear rate at port No.2 is higher than at port No.1, resulting in a lower non-Newtonian viscosity. The overall viscosity during systole is lower than during diastole as the shear rate during systole is high. At the peak of systole the non-Newtonian viscosity is 0.037 poise which is the infinite-shear-rate viscosity measured using the dog's blood with a cone and plate viscometer. Near the zero shear rate the non-Newtonian viscosity is between 0.08-0.14 poise which is 2-3 times the infinite-shear-rate viscosity. The non-Newtonian viscosity increases during the late decelerating part of systole which is due to the drop in shear rate and subsequent change of shear rate from a positive to a negative value. Due to the higher systolic decelerating slope, at the end of systole and at the beginning of diastole the shear rate for port No.2 is lower than for port No.1, which causes a local high value of the non-Newtonian viscosity.

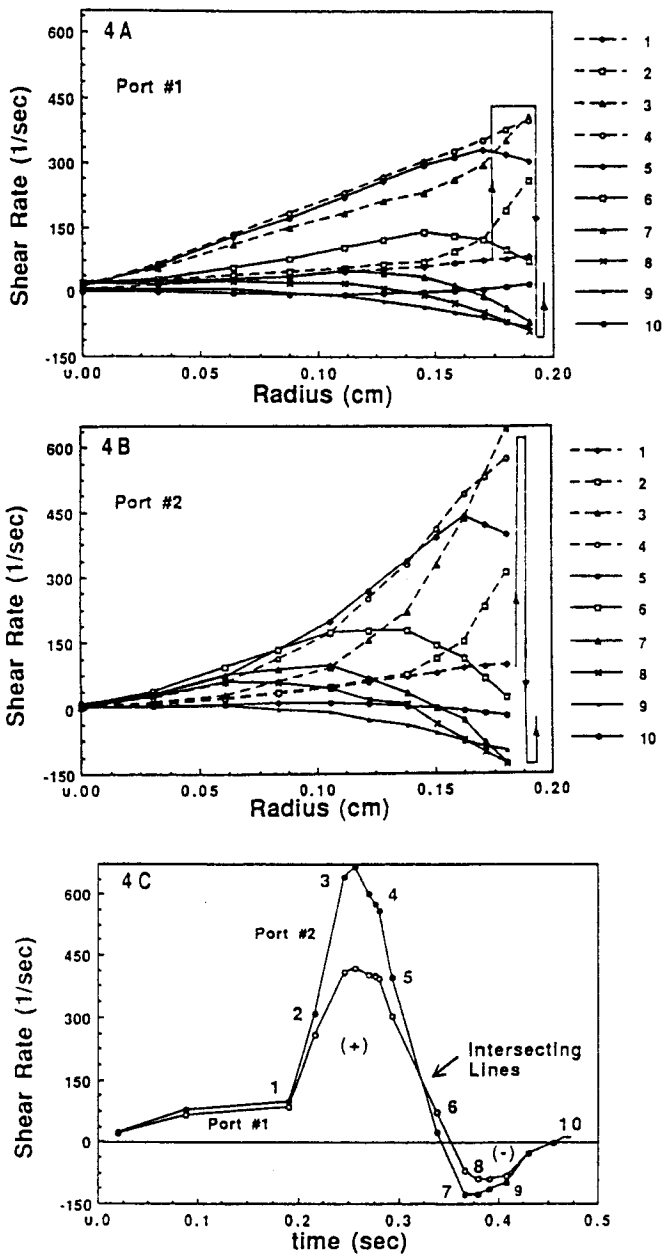

FIG. 4 Radial shear rate distribution for different time steps along a pulse cycle at port No. 1 (Fig. 4A) and at port No. 2 (Fig. 4B). Temporal variation of wall shear rate distribution at port No. 1 and at port No. 2 (Fig. 4C).

Figure 6 illustrates the oscillating shear stress along the arterial wall. During the systolic acceleration the wall shear stress increases from a value of 0 to +34 dynes /cm^2, followed by a drop to a value of -9 dynes /cm^2 during the decelerating phase of flow. Subsequently, there is a rise of shear stress to a positive value of 2 dynes /cm^2. The shear stress obtained along the wall shows the combined effect of instantaneous wall shear rate and the non-Newtonian viscosity.

The pressure drop calculated for different pressure formulations are presented in Fig. 7. Curves A-C represent the pressure drop for a parabolic inlet condition whereas curve D is for an uniform inlet velocity profile. Penalty (discontinuous) pressure approximation was performed with both linear (curve A for local and curve B for global pressure basis function) and bilinear pressure formulations

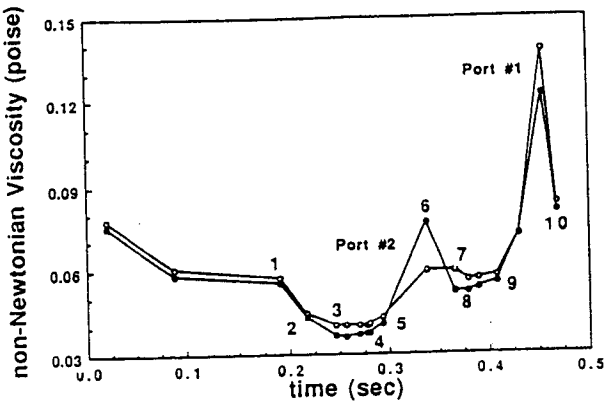

FIG. 5 Temporal variation of non-Newtonian viscosity at wall for port No. 1 and at port No. 2.

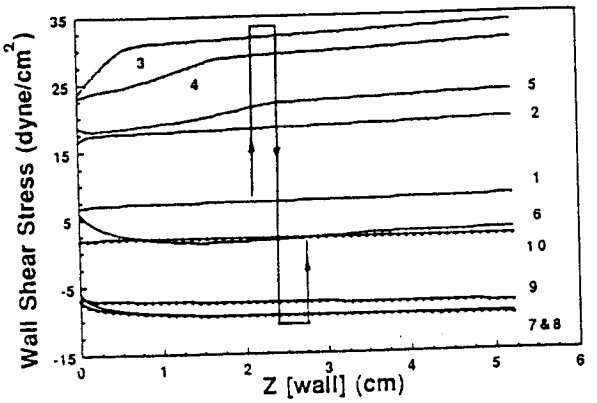

FIG. 6 Wall shear rate distribution for different time steps along a pulse cycle between port No. 1 and port No. 2.

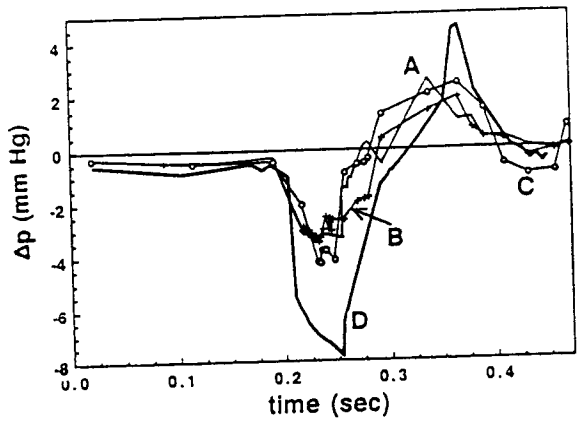

FIG. 7 Temporal variation of pressure drop at wall between port No. 1 and port No. 2 along a pulse cycle. Curve A-C: Parabolic inlet and Curve D: Uniform inlet. Curve C and D: Penalty- bilinear pressure formulation. Curve A and B: Penalty- linear pressure formulation with local [for A] and global [for B] basis function.

(curves C and D). For the bilinear pressure formulation, the maximum pressure drop of -7.9 mm Hg (represented by downward spike) and rise of +4.5 mm Hg (represented by upward spike) are obtained for a uniform flow inlet condition whereas for the parabolic flow the drop is -4.3 mm Hg and the rise is +2.4 mm Hg. The pressure drop for the linear pressure approximation for both local (-3.6 mm Hg) and global (-3.5 mm Hg) basis functions are less in comparison to the bilinear case. During the acceleration part of the flow the maximum pressure drop is obtained at t= 0.254 sec whereas a subsequent rise in pressure is noted for a decelerating flow at t= 0.367 sec, which is followed by a drop in pressure to a zero value. From Fig. 2B, a peak positive velocity is obtained at t= 0.277 sec whereas a peak negative value is obtained at t= 0.408 sec. This clearly indicates some small phase-lag between pressure and velocity waves and also a hysteresis effect between pressure drop and velocity. The dimensionless frequency parameter [α= 0.5 D $(\omega/\nu)0.5$] for the dog was 3.7.

SUMMARY

The observations made in the present study are summarized as follows:

1) Knowing the *in-vivo* velocity pulse by a Doppler flow cuff method, the physiological pressure drop was calculated for a normal femoral artery of dog. The prediction of pressure drop has a potential application from the medical diagnostic point of view since prone sites of blockage or stenosis may be identified without invasive means. The hydrodynamic study should help to understand the mechanism of the development of blockage which is site-specific in nature.

2) The prediction of *in-vivo* pressure drop will be within the two limits of instantaneous input flow conditions: uniform and parabolic. Due to the developing nature of flow the prediction will be more closer to the uniform inlet flow condition case than parabolic.

3) The mild taper of the artery causes a higher magnitude of oscillating wall shear rate during both systole and diastole of a pulse cycle. Furthermore, the steeper gradient of wall shear rate due to taper affects not only the non-Newtonian viscosity and shear stress but also the pressure.

REFERENCES

1. Nichols, W. W. and O'Rourke, M. F., *McDonald's Blood Flow in Arteries*, (3rd Ed.), Chapter 5, Edward Arnold (Publisher), 1990.
2. Womersley, J., R.,"Method for the Calculation of Velocity, Rate of Flow and Viscous Drag in Arteries when the Pressure Gradient is known," *J. Physiol.*, 127, 1955, 553-563.
3. Ling, S. C., Atabek, H. B. and Carmody, J. J.,"Pulsatile Flow in Arteries," *Proc. of 12th Int. Cong. of Applied Mechanics*," Springer-Verlag (Publisher), 1968, 277-291.
4. Back, L. H., Back, M.R., Kwack, E.Y. and Crawford, D. W., "Flow measurements in a human femoral artery model with reverse lumen curvature," *ASME J. Biomech. Engrg.*, 110, 1988, 300-309.
5. Talbot, L., and Berger, S. A.,"Fluid-Mechanical Aspects of the Human Circulation," *American Scientist*, 62, 1974, 671-682.
6. Mann, D. E. and Tarbell, J. M., "Flow of Non- Newtonian Blood Analog Fluid in Rigid Curved and Straight Artery Models," *Biorheology*, 27, 1990, 711-733.
7. Liepsch, D., Thurston, G. and Lee, M.,"Studies of Fluids Simulating Blood-like Rheological Properties and Application in Models of Arterial Branches," *Biorheology*, 28, 1991, 39-52.
8. Cho, Y.I. and Kensey, K.R., "Effects of the Non-Newtonian Viscosity of Blood on Flows in a Diseased Arterial Vessel: Part 1, Steady flows," *Biorheology*, 28, 1991, 241-262.
9. Banerjee, R.K., Cho, Y.I. and Kensey, K.R., "Effect of the Non-Newtonian Viscosity of Blood on Steady and Pulsatile Flow in Stenosed Arteries," *Advances in Bioengineering, ASME*, 1991,103-106.
10. Baker, A.J., *Finite Element Computational Fluid Mechanics*, Hemisphere Publishing Corp., 1983.
11. FIDAP Manual [1991], Fluid Dynamics International, Inc., Evanston, Illinois.
12. Walburn, F. J. and Schneck, D. J.,"A Constitutive Equation for a Whole blood Model," *Biorheology*, 21, 1976, 201-210.
13. Chien, S., Usami, S., Dellenback, R. J. and Bryant, C. A., "Comparative Hemorheology- Hematological Implications of Specie. Differences in Blood Viscosity," Biorheology, 8, 1971, 35-57.